A Device for Study of Polymer Crystallization Kinetics via Real-Time Image Analysis of Small Angle Light Scattering

WAYNE T. CULBERSON and MARTIN R. TANT*

Research Laboratories, Eastman Chemical Company, Kingsport, TN 37662

SYNOPSIS

A two-dimensional position-sensitive detector for real-time small-angle light scattering (RTSALS) of polymers is described. The device performs real-time image analysis of the evolving light-scattering pattern during crystallization. Such an approach provides a means of simultaneously measuring the rate of spherulite growth and the overall rate of crystallization, allowing calculation of nucleation density and/or rate. Although separation of nucleation effects from growth effects typically requires the application of two different experimental techniques, this device is unique in that it allows these two effects to be easily separated using only time-dependent light-scattering data. The device incorporates a CCD camera, a personal computer, and an imaging board as its major hardware components. Software designed specifically for this application performs real-time analysis of the light-scattering pattern at a rate of 1–3 images per second, thus allowing study of even moderately rapidly crystallizing polymers. (More recent software modifications have resulted in a speed enhancement to 5 images per s and further improvement is expected.) Intensities at various scattering and azimuthal angles are plotted at each time. In addition, the average spherulite radius is calculated and plotted. Application of the device is illustrated by measuring the spherulite growth rate of poly(ethylene terephthalate) as a function of temperature. © 1993 John Wiley & Sons, Inc.

INTRODUCTION

Obtaining an understanding of polymer crystallization kinetics and its effect on crystalline morphology is of paramount importance for the design of the materials and processes needed to produce polymer products with optimum mechanical and optical properties. The most widely used techniques for studying crystallization kinetics are differential scanning calorimetry (DSC) and hot-stage optical microscopy. DSC is limited by the fact that it often cannot be applied in the temperature regime where crystallization is rapid. It gives only bulk crystallization rate and no direct morphological information. Many studies of crystallizatilon kinetics also utilize hot-stage optical microscopy to obtain radial growth rate data for spherulities. This information, in combination with bulk crystallization rates obtained by DSC, gives a more complete description of the crystallization process. However, the microscopy technique can be extremely tedious since the radius of a spherulite must be physically measured as a function of time. If the spherulites are still small at the completion of the crystallization process, as is the case for many common polymers, growth rate data might be obtainable only at the very end of the process due to the practical limitations of magnification power. In some cases the spherulites may never reach a measurable size. Thus, obtaining a good understanding of the crystallization behavior of a polymer as a function of temperature and other variables using these standard techniques may require a great deal of time devoted to meticulous experimental work.

More than thirty years ago, Stein and coworkers[1-3] began to apply the technique of small-angle light scattering (SALS) to the study of polymer crystalline morphology. Stein and Rhodes[4] derived the equations for scattering from anisotropic spherulites and developed the photographic SALS

* To whom correspondence should be addressed.

Journal of Applied Polymer Science, Vol. 47, 395–405 (1993)
 CCC 0021-8995/93/030395-11

method. These equations were slightly modified later by Samuels.[5] Photographic SALS proved to be a simple and rapid technique for determining spherulite size as well as for obtaining information concerning other aspects of crystalline structure such as type of structure (e.g., spherulitic vs. rod-like structure), orientation of polymer chains within the structure, etc. Several researchers have utilized SALS to follow the crystallization kinetics and spherulite growth of polymers.[6–11] These workers typically utilized photographic techniques in which photographs of the SALS patterns were taken as a function of time during the crystallization process and saved for later analysis. In 1971 van Antwerpen and van Krevelen[12,13] reported the development of a small-angle light-scattering device that operated dynamically and was used to study the crystallization kinetics of poly(ethylene terephthalate) (PET). Their experimental apparatus utilized a photocell that physically moved along a specified azimuthal angle to measure the intensity of the scattered light as a function of both scattering angle and time. The recent development of high-quality video cameras and electronic image analysis capabilities has led to their application for the analysis of polymer SALS patterns. Stein and coworkers[14–17] have used this approach to obtain data concerning crystalline morphology, melting behavior, spherulite growth rate, and bulk crystallization rate. Their device utilizes a 50 × 50 pixel array and can perform one scan every 10 s. The device was designed primarily for studies directed at quantitative analysis of the total light-scattering pattern. But it has been used to study melting as well as the crystallization kinetics of relatively slowly crystallizing systems.[17] A similar device developed by Effler, Lewis, and Fellers[18] has a 249 × 236 pixel array and can perform one scan every 15 s. This device has not been utilized to study crystallization kinetics. Both of these devices store the entire array of intensity data for later analysis.

Here we describe a real-time SALS device (RTSALS) which performs data analysis during crystallization, making the storage of large arrays unnecessary. A 512 × 480 pixel array is utilized. Scans can be performed at the rate of 1–3 per s. (More recent software modifications have resulted in a speed enhancement to 5 scans per s and significant further improvement is likely.) These rates of data acquisition and processing thus make the device useful for study of even moderately rapidly crystallizing materials. Further data analysis is unnecessary. Data are reported here that demonstrate the application of the apparatus to measure the temperature-dependent spherulite growth rate of poly(ethylene terephthalate).

BACKGROUND

In this section we will briefly describe the scattering of light by semicrystalline polymers and how the technique of small-angle light scattering can be utilized to study polymer superstructure, spherulite growth rates, and bulk crystallization rates. This is not intended to be a complete review of the subject since several such reviews are available.[19–22] We will consider the basic structure of spherulites present in many semicrystalline polymers, the light scattering caused by these structures, as well as what information can be gained about spherulitic structures from light-scattering experiments.

When electromagnetic radiation of the wavelength of light propagates through a nonabsorbing medium, the intensity of the incident beam is observed to decrease due to the phenomenon of scattering. This scattering of light results from local variations in the dielectric tensor of the medium. Such variations may arise from isotropic or anisotropic heterogeneities, which, for bulk polymers, may be due to several different sources, such as: (i) density fluctuations; (ii) fluctuations in local anisotropy that correlate with the structure or orientation; (iii) fluctuations in local anisotropy that do not correlate with local structure or orientation; and (iv) optical rotation. Density fluctuations lead to isotropic scattering while the others result in anisotropic scattering. For semicrystalline polymers, the scattering of interest is that resulting from fluctuations in local anisotropy that do correlate with structure or orientation. The other causes, while they certainly occur to some extent, do not contribute to our understanding of polymer superstructure and will not be considered in this discussion.

During crystallization, lamellar crystals typically grow from a heterogeneous nucleus, first forming a sheaf-like structure that gradually transforms to a spherically-shaped structure, the spherulite. The spherulitic structure develops from lamellae that grow radially through chain folding, branching as they grow outward.[23] Therefore, the polymer chains are usually oriented tangentially within the spherulite. (There may be some variations to this typical structure as will be described later.) Since the valence electrons within a polymer chain are more easily polarized along the bond than perpendicular to it, the preferred tangential orientation of the chains within the spherulite results in these structures being optically anisotropic.

In the small-angle light-scattering apparatus usually used for studying semicrystalline polymers, plane-polarized light (0.6328 μ) emitted by a helium–neon laser is passed directly through the sample of interest. It is important that the sample be thin enough so that at least 75% of the incident light is transmitted, thus minimizing the effects of secondary scattering. Both the transmitted and scattered light then pass through a polarizer whose polarization direction may be 90° to that of the laser (H_v scattering) or parallel to that of the laser (V_v scattering). In the photographic SALS technique, the scattered light is projected upon photographic film to obtain an image. As mentioned earlier, other detection methods can be used to determine scattered intensity as a function of the azimuthal and scattering angles.

The typical H_v pattern resulting from light scattering by polymer spherulites is the so-called four-leaf clover in which the lobes are oriented at ±45° to the polarizer and analyzer. It is the tangential component of spherulite polarizability which gives rise to this pattern. Many workers have observed that the lobes of the scattering pattern are sometimes oriented at 0° and 90° instead of the more usual ±45°.[7,11,24,25] These "unusual" patterns, as they are referred to, suggest that the chains are oriented somewhere nearer 45° to the radial direction rather than the more typical 90°.[24] In some instances a change from an unusual to a usual scattering pattern has been observed to occur upon annealing.[25] In addition, some researchers have observed, as have we, that an unusual pattern appearing during initial growth may change to a usual pattern at a later stage in the growth process.[8] These observations, their implications for polymer morphology, and the controlling parameters are not well understood.

Light scattering results are typically analyzed by using either a model approach, where a model is assumed for the morphology and the expected scattering is calculated, or a statistical approach, where the scattering is directly analyzed to give information about the system in terms of isotropic or anisotropic fluctuations, persistence lengths, or correlation functions. The statistical approach is used when a reasonable morphological model for the system cannot be envisaged, as occurs for more disordered systems. For systems that display more order, such as the semicrystalline polymers having spherulitic superstructures of interest here, the model approach is used. Hence we will consider only the results of this approach.

Without giving details of the derivation,[4,5] the intensity of H_v and V_v scattering resulting from a system of model spheres having polarizabilities α_r and α_t in the radial and tangential directions, respectively, imbedded in an isotropic matrix with polarizability α_s, is given by

$$I(V_v) = A\rho^2 V_o^2 \left(\frac{3}{U^3}\right)^2 \Big\{(\alpha_t - \alpha_s) \times (2\sin U - U\cos U - SiU) + (\alpha_r - \alpha_s) \times (SiU - \sin U) + (\alpha_r - \alpha_t)\left[\frac{\cos^2(\theta/2)}{\cos\theta}\right] \times \cos^2\mu(4\sin U - U\cos U - 3SiU)\Big\}^2 \quad (1)$$

and

$$I(H_v) = A\rho_2 V_o^2 \left(\frac{3}{U^3}\right)^2 \times \left\{(\alpha_r - \alpha_t)\left[\frac{\cos^2(\theta/2)}{\cos\theta}\right]\sin\mu\cos\mu \times (4\sin U - U\cos U - 3SiU)\right\}^2 \quad (2)$$

where

A = proportionality constant

ρ = geometric polarization correction term,

$$\rho = \cos\theta(\cos^2\theta + \sin^2\theta\cos^2\mu)^{-1/2} \quad \text{for } V_v \quad (3)$$

$$\rho = \cos\theta(\cos 2\theta + \sin^2\theta\sin^2\mu)^{-1/2} \quad \text{for } H_v \quad (4)$$

V_0 = volume of the spherulite

$\alpha_t, \alpha_r, \alpha_s$ = tangential, radial, and average surrounding polarizabilities

$U = 4\pi R_o/\lambda \sin(\theta/2)$ where R_o is the radius of the spherulite and θ is the radial scattering angle

μ = azimuthal scattering angle taken as zero along the vertical for a vertically oriented polarizer

and

$$S_i U = \int_0^U \frac{\sin x}{x}\,dx. \quad (5)$$

Several deviations between experimental and predicted intensity profiles do arise, however, and these

have been identified and treated quantitatively by Stein and coworkers. Deviations at low angles result from interspherulitic interference and spherulite impingement,[15,16,26,27] while density and anisotropy fluctuations within spherulites are typically responsible for wide angle deviations.[16,28,29] It should also be noted that the equation for V_v scattering includes contributions for both isotropic and anisotropic scattering while that for H_v scattering includes only the anisotropy of the spherulite. Thus the H_v scattering pattern typically contains the most useful information for spherulitic scattering, although Samuels[5] has stressed that the importance of V_v scattering is often not recognized.

It should be mentioned that although eq. (2) for H_v scattering predicts no scattered intensity for isotropic spheres, Meeten and Navard[30] have recently shown that an H_v pattern is also observed in this case. The H_v pattern for isotropic spheres is, in fact, the typical four-leaf clover observed for anisotropic spheres with higher order maxima occurring as well. The effect of increasing spherulite anisotropy is to increase the intensity of the first order scattering maximum while shifting this maximum to greater scattering angles. Therefore, spherulitic H_v scattering consists of a four-lobed pattern corresponding to the first order intensity maximum with negligible intensity in the higher orders.

The angle of maximum scattered intensity from H_v scattering is related to the size of the spherulites. It can be shown[4] that for anisotropic spherulites this maximum occurs at

$$U_{\max} = \frac{4R_o\pi}{\lambda_m} \sin\left(\frac{\theta_{\max}}{2}\right) = 4.09 \qquad (6)$$

where λ_m is the wavelength of light and $\theta_{\max}$ is the angle of maximum scattered intensity, both measured in the medium. Van Antwerpen[12] has shown that values of these two variables measured in air without correction for refraction give spherulite radius results that are well within the error of the measurement. This relationship is utilized in the present work to determine spherulite radius as a function of time. From these data it is then a simple matter to calculate the spherulite growth rate at any stage during the crystallization process.

There are several factors of which one should be aware when utilizing this technique for determining average spherulite size. First, the value of the spherulite radius determined from eq. (6) is heavily weighted toward larger spherulites due to the V^2 term in eq. (2). Second, as spherulite size increases, accurate measurement of the scattering angle becomes increasingly important. In fact, for the experimental set-up used in our work, measurement of average spherulite radii above 5–6 μ is questionable. Finally, as mentioned above, it has been pointed out by Meeten and Navard[30] that $U_{\max}$ is a function of both spherulite size and spherulite anisotropy. For isotropic spheres $U_{\max}$ is about 2.7, while for anisotropic spheres $U_{\max}$ approaches 4.09. For spherulites having the anisotropy of PET spherulites and in the size range studied by the device described here, $U_{\max}$ is about 4.09.

Knowing that the spherulite radius can be obtained from the scattering angle of maximum intensity, it is obvious that the spherulite radius can be determined as a function of time and, therefore, the spherulite growth rate can be obtained by monitoring this angle during crystallization. The spherulite growth rate may be represented by the well-known Turnbull–Fisher equation[31]

$$\ln G = \ln G_o - \frac{\Delta E}{kT} - \frac{\Delta F^*}{kT} \qquad (7)$$

where G is the linear growth rate, ΔE is the free energy of activation for the transport of units across the phase boundary, ΔF^* is the free energy of activation for the formation of a nucleus of critical size, k is the Boltzmann constant, and T is absolute temperature. There are several methods for determining the various constants, but these will not be discussed here.

To obtain a complete understanding of the kinetics of crystallization it is necessary that both bulk crystallization rate and spherulite growth rate be determined. While it is common to obtain the data for each from different experiments under (presumably) the same conditions, it is possible to obtain both bulk crystallization rate and spherulite growth rate simultaneously from a RTSALS experiment. It is thus assured that both bulk crystallization rates and spherulite growth rates are obtained on a sample that has experienced precisely the same temperature history. The bulk crystallization rate is typically modeled by the Avrami equation,[32] i.e.,

$$X_c(t) = 1 - \exp(-Kt^n) \qquad (8)$$

where $X_c(t)$ is the volume fraction of crystals at time t; K is a rate constant that includes the temperature dependent terms, including nucleation and diffusion rates; and n is the Avrami constant, a constant which depends upon the types of processes

occurring during nucleation and growth. The constants K and n are typically determined from bulk crystallization data obtained at different temperatures. The change in percent crystallinity during crystallization may be monitored by following the total intensity of depolarized scattered light.[33,34] Knowing the scattered light intensity from the fully crystallized polymer, the crystallization halftime is located where the overall intensity is one-half that when fully crystallized.

If spherulitic impingement occurs, the nucleation density, N, can be calculated from the equation

$$N = \frac{3x}{4\pi R_{\max}^3} \tag{9}$$

where $x \simeq 1$. If it is assumed that nucleation results in the development of three-dimensional spherulites and that spherulite growth is linear with time, the nucleation density may be calculated from the equation

$$N = \frac{3K}{4\pi G^3}. \tag{10}$$

Knowledge of the value of K from the Avrami equation and G, the spherulite growth rate, thus allows calculation of the nucleation density.

In this paper we focus primarily on the measurement of spherulite growth rates, since quantitative measurement of total depolarized scattered light, and thus bulk crystallization rates, only recently became possible. Future work will focus on combining both capabilities of the SALS device.

EQUIPMENT DESIGN AND IMAGE ANALYSIS

SALS Device

In the device used in this work, polarized monochromatic light having a wavelength of 0.6328 μ is passed through a thin polymer film (the sample), through a crossed polarizer (H_v scattering), and onto a diffusing screen. In a darkened room, the light scattered by the sample is projected onto the diffusing screen to form a pattern that is visible to the human eye and to the video camera. The analog position-dependent intensities which form the image are captured by the camera and are fed to the imaging board in the computer where they are digitized. The digital image is placed in a frame buffer where it is analyzed by the image processor and computer. The live or stored image is displayed on the image monitor and a hard copy of any image being viewed can be made by the videographic printer. A VCR is also connected to the video output of the imaging board so that an experimental run may be recorded for future reference. Control of the experiment and the display of data is accomplished through a menu-driven interface that utilizes both video monitors, the keyboard, and the mouse.

The polymer film is placed in a modified microscopy hot stage maintained at the desired crystallization temperature. A low-mass sample holder, a 1″ × 5″ piece of 0.010″ thick paper cut from an index card, is used to allow rapid temperature equilibration. A $\frac{3}{4}$″ diameter hole is cut near one end of the paper strip and a glass cover slip glued over the hole. The polymer is then melt pressed between this cover slip and another cover slip at a specified temperature and time. The sample can be inserted into the hot stage directly from the melt or quenched to room temperature and then inserted to investigate crystallization from the glass. The hot stage, which can operate isothermally or nonisothermally, is calibrated using melting point standards.

During an experiment, the images are digitized and immediately processed at a rate of 1–3 images per s depending on the analysis method. (Scan rates have recently been improved to 5 per s by software modification, and a further fourfold enhancement appears to be attainable with current hardware.) The analysis objective is to obtain spherulite radius and azimuthal intensity profiles as a function of time. At each sample point, the time, radius, and several azimuthal intensity values are written to a computer file. The intensity values represent the azimuthal angles from 0°–90° in 5° increments taken at the radius of peak intensity and averaged over the four quadrants. At the end of the run the data are plotted for viewing. The time-dependent radius and intensities at various azimuthal angles are plotted separately on the image monitor. A mouse-controlled cursor is used to select regions for data review, data pruning, and slope calculation.

Since absolute intensity values are required for the determination of bulk crystallization rates and since the dynamic range of light intensities in these experiments is large, there were special considerations regarding the camera gain and/or lens aperture. Because of the high contrast image and the very large change in absolute total intensity during the experiment, the automatic gain control of the camera did not perform adequately. A new lens system was designed in which the camera gain is fixed and the lens aperture set via computer control of a

stepping motor. Digital-to-analog capability was added to the computer and a mechanical system and software were designed to allow control of the lens f-stop and scaling of the intensity values. The aperture is set to full open at the beginning of the experiment due to the very low intensity, and is gradually closed as crystallization proceeds and the image becomes more intense. Calibration is accomplished by viewing a constant and uniformly lighted surface while each position of the aperture is visited. The intensity is measured and the scale factor calculated. Although this arrangement functions relatively well, the fact that it is a mechanical system has led to certain problems. A potentially much better approach, and one that is being pursued, is to use a camera with computer-controllable integration time that can be decreased as the image becomes more intense. These cameras, which are just now becoming available, offer precise and repeatable intensity control because the integration time is based on a crystal clock.

Image Analysis

It is assumed that the scattering pattern will take the form of a four-leaf clover with each of the four lobes falling on either ±45° or 0°–90° orientations. The spherulite radius is inversely related to the distance from the center of the pattern to the point of peak intensity in the lobes according to eq. (6). In theory the spatial distribution of intensities in the vicinity of a lobe could be represented by smooth circular contour lines. In practice this is not true. Equal intensity contour lines are quite noisy and distorted due to laser speckle. Thus most of the image analysis work involves finding the lobe peak. There are presently two methods of peak lobe detection. One method profiles the image and the other method uses a vector approach.

Profile Method

The two main steps of the profile method are: (i) eliminate background, i.e., only the brighter pixels are considered and (ii) profile (i.e., sum rows/columns) the intensities in the x and y directions to map the noisy two-dimensional image array to two relatively smooth one-dimensional arrays that should each have two peaks. Each peak represents the location of the maximum lobe intensity. It is assumed that the lobes have a ±45° orientation. The lobe radius is then calculated as $0.5*(\Delta X^2 + \Delta Y^2)^{1/2}$ where ΔX and ΔY represent the distance between peaks in the respective one dimensional arrays. Step (i) acknowledges the fact that the lobes will be brighter than the background, and step (ii) attempts to handle the intensity fluctuations that occur about the lobe. Figure 1 illustrates schematically the basics of the profile method.

Vector Method

In the vector method, intensity profiles are taken along vectors that radiate out from the center of the pattern at angles of ±45° or 0°–90°, as illustrated in Figure 2. The four profiles are then averaged. Determination of the lobe peak directly from this raw-average intensity profile is not possible due to the large amount of noise. Even after significant smoothing, the location of the lobe peak was found to result in quite noisy spherulite growth curves primarily due to the breadth of the lobe peak. Thus, the approach taken was to integrate the lobe peak as shown in Figure 2 and to determine the lobe peak using a center-of-mass calculation. This procedure was found to result in very smooth spherulite growth curves, and, as will be shown later, very good agreement with results of the profile method.

The vector method also provides the capability to change the directions of the four vectors to azimuthal angles of 0°–90° (unusual spherulites) from ±45° (usual spherulites) during an experiment. This change is performed using a designated mouse button that toggles the vector directions between these two options, thus allowing the study of systems that change from one to the other during a single crystallization experiment.

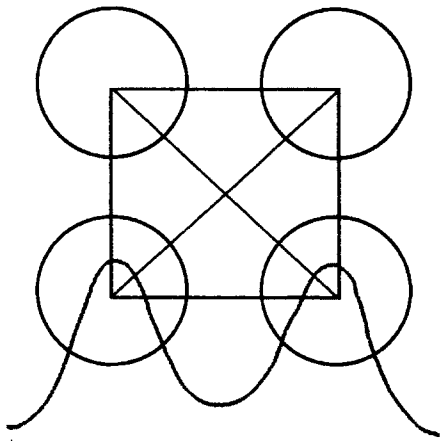

Figure 1 Illustration of the Profile Method used to determine lobe peak locations.

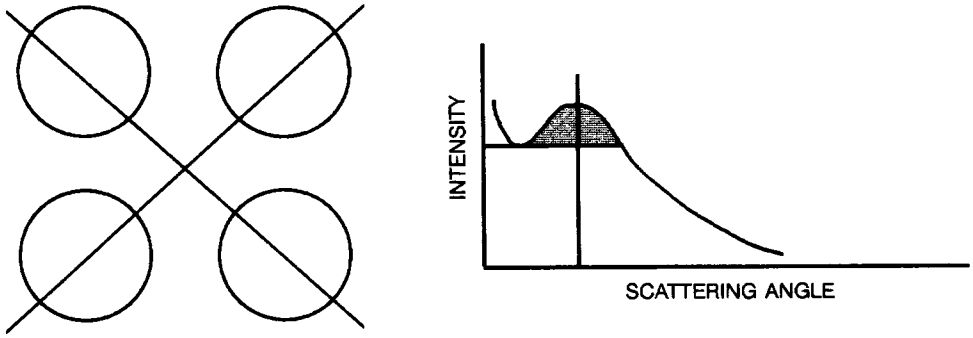

Vector (3 Scans/Sec)

1. Sum Intensities Along 4 Vectors Radiating Out From Center Through Lobes (±45° or 0-90°)
2. Smooth Intensity Profile
3. Locate Intensity Minimum Between Center of Pattern and Intensity Maximum
4. Perform Center of Mass Calculation on Peak Area Between Smoothed Curve and Intensity Minimum Found in Step 3
5. Calculate Spherulite Radius

Figure 2 Illustration of the Vector Method used to determine lobe peak locations.

DEMONSTRATION OF SALS DEVICE

An example of a scattering pattern that is projected onto the diffuser is shown in Figure 3(a). This pattern was imaged by the camera/lens system, digitized and displayed by the imaging board. Figure 3(b) shows this image after considerable smoothing and the addition of equal intensity contour lines. There are no concentric contour lines without the smoothing. Also, not all images are this good.

Figure 4 shows plots displayed on the image monitor after an experiment. The data represented by these plots reside in computer files so they may be replicated at any time. The upper plot shows the spherulite radius vs. time, and the lower plot shows intensity vs. time at several different azimuthal angles. A mouse-controlled vertical bar is overlaid on these plots with the position of the bar representing a particular sampling time. The radius and 45° intensity associated with this sampling time are displayed. The equation for the line between selected radius data points is shown in the lower right corner of the radius plot (slope = growth rate), and the time to half maximum of the 45° intensities is shown in the lower right corner of the intensity plot. These values are the primary information of interest obtained from a SALS experiment directed at determining crystallization kinetics.

It is often desirable to plot several growth-rate curves on one graph to compare growth rates of different samples. This capability is included as a menu item. Its application is illustrated by Figure 5 which shows the results of two PET crystallization experiments plotted together where one of the samples contains sodium and the other does not. Sodium, a nucleating agent for PET, creates more spherulite growth sites. Spherulitic impingement thus occurs at an earlier time, resulting in a smaller maximum spherulite radius. Figure 5 clearly shows this effect, i.e., spherulites in the material containing sodium reach a smaller maximum radius than the spherulites in the material that does not contain sodium. This is just one example of the usefulness and practical convenience of the real-time SALS device for studying polymer crystallization.

To further illustrate the application of the RTSALS device, the effect of temperature on the spherulite growth rate of PET having a number-average molecular weight of 24700 is shown in Figure 6. Crystallization experiments were conducted from the glass. Each point represents the mean of experiments on at least five different samples. The error bars indicate 95% confidence intervals. As expected, the growth rate curve is parabolically shaped with a maximum about midway between the T_g and T_m. This, of course, is well-known behavior and results from the rate-limiting steps of diffusion at lower

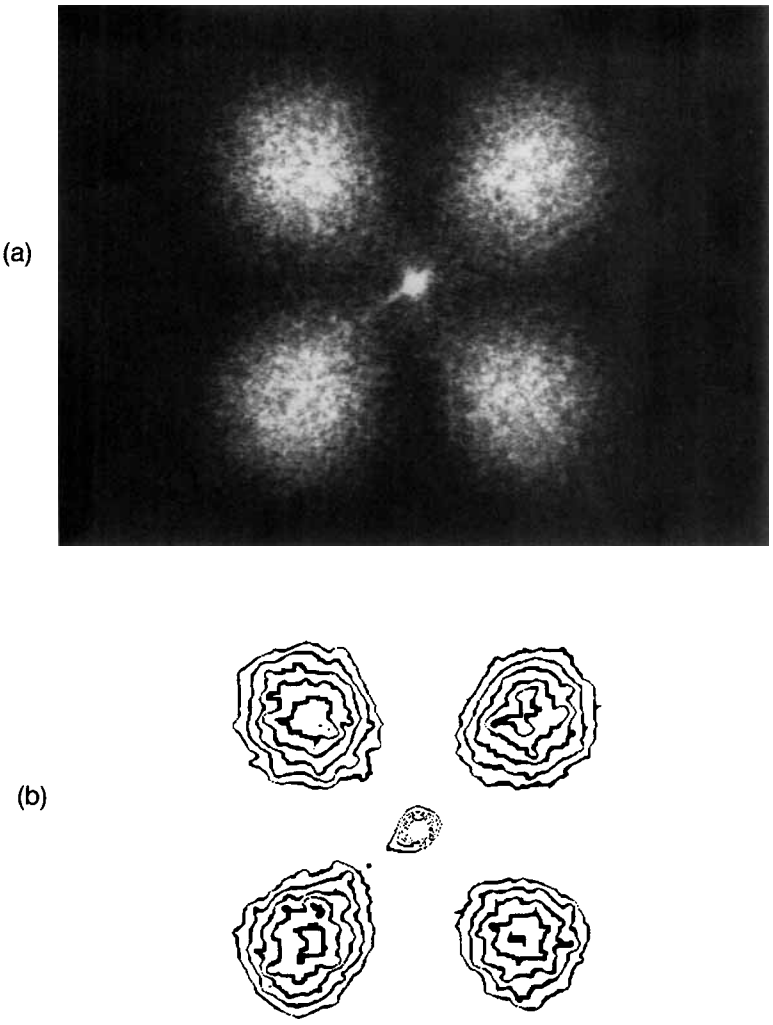

Figure 3 Typical H_v scattering pattern for poly(ethylene terephthalate). (a) Pattern was imaged by the camera/lens system, digitized, and displayed by the videographic printer. (b) Same image after 16 smoothing operations and the addition of equal intensity contour lines.

temperatures and nucleation at higher temperatures. The smooth curve drawn through the data is optimized based on the Turnbull-Fisher equation and will be thoroughly addressed in a future paper. The equation for this curve is

$$\ln G = \ln (5.99 \times 10^5) - 4100/R(15.6 + T - T_g) - 224T_m^2/T^2(T_m - T) \quad (11)$$

where R is the universal gas constant (8.31 J/mol-K), T is the crystallization temperature (K), T_g is the glass transition temperature (353 K), and T_m is the melting point (523 K).

If the profile and vector methods properly locate the scattering maximum, the spherulite radii determined by the two methods should be the same. To check this, the changing light-scattering pattern during a crystallization experiment was analyzed using the vector method while recording the pattern with the VCR. The videotape of the evolving SALS pattern was then replayed and analyzed using the profile method. The spherulite growth curves obtained by these two methods are compared in Figure 7. Clearly they are essentially the same except at the largest spherulite size (smallest angles). At smaller angles the calculated spherulite radius becomes much more sensitive to angle, requiring more

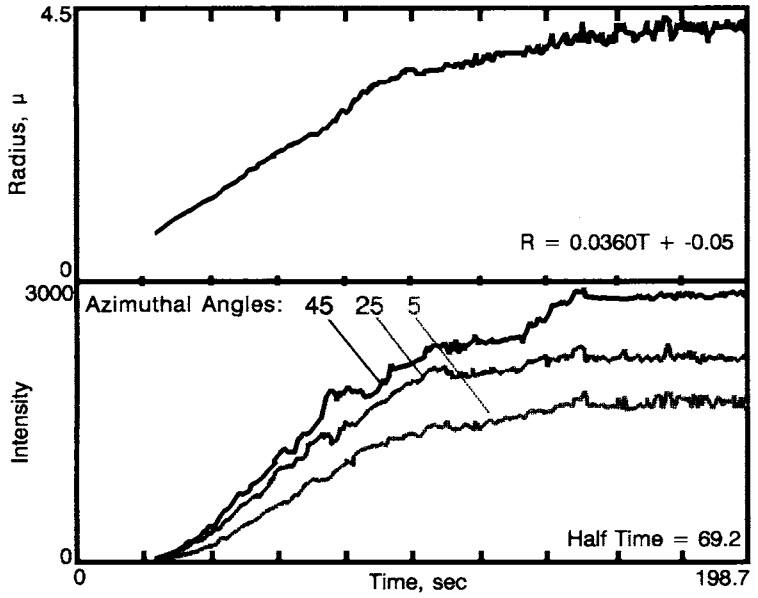

Figure 4 Example of plots displayed by the image monitor following a crystallization experiment. The upper plot shows the average spherulite radius as a function of time. Lower curves show the intensity at the lobe peak as a function of time at several azimuthal angles. The equation displayed in the upper portion represents a least squares fit of the data during the early part of the crystallization. The slope of this curve therefore gives the spherulite growth rate in μ/s.

accurate measurement of the angle. The deviation between the two curves at small scattering angles may be the result of this greater sensitivity. However, even with this small deviation, the agreement between the two curves is quite satisfying.

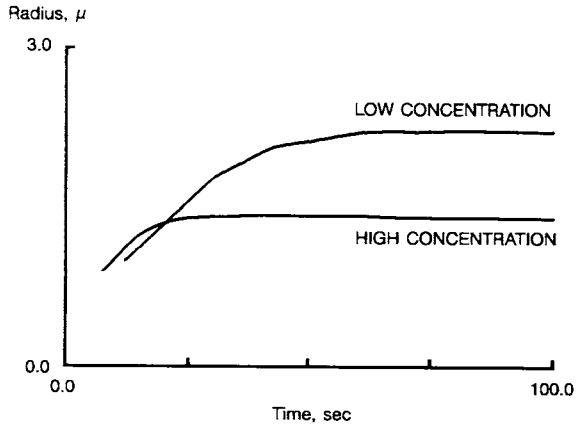

Figure 5 Illustration of the effect of nucleation density on spherulite growth curves. The samples were cut from PET molded parisons, melted at 280°C for 20 seconds, and then crystallized from the melt at 130°C. The lower two curves were obtained for material that contained sodium while the upper two curves were obtained from material not containing sodium.

CONCLUSIONS

A small-angle light-scattering device that utilizes real-time image analysis has been designed and constructed for determining the spherulite growth rate, bulk crystallization rate, and nucleation density of

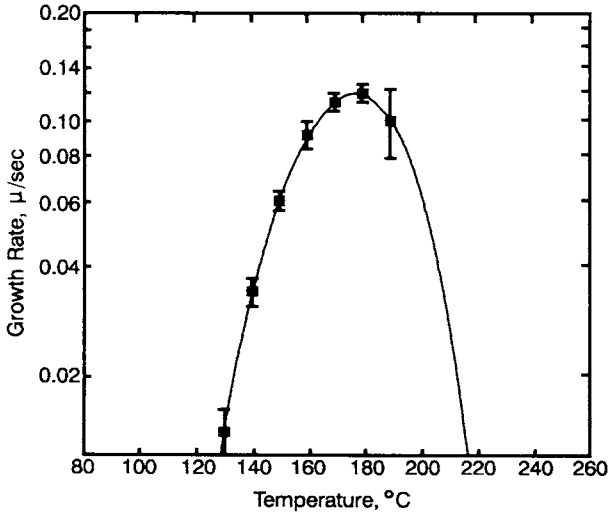

Figure 6 Effect of temperature on the spherulite growth rate for poly(ethylene terephthalate) having a number-average molecular weight of 24700.

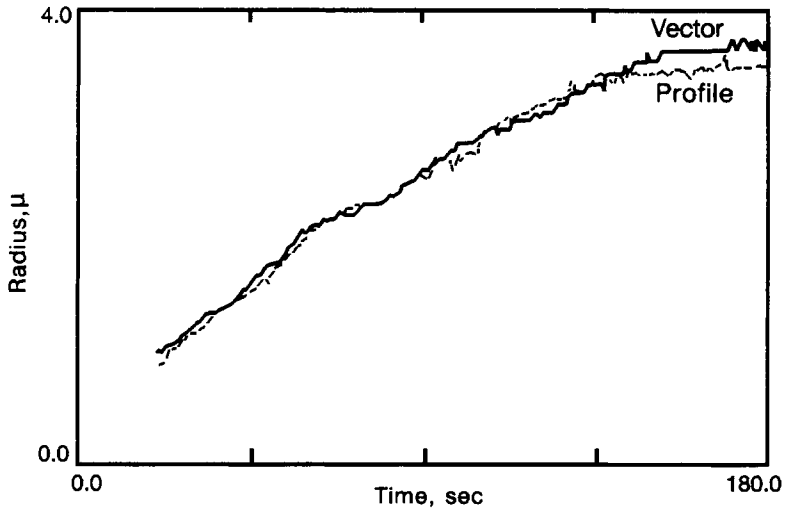

Figure 7 Comparison of spherulite growth curves obtained for the same crystallization experiment using the two available programs PROFILE and VECTOR. The data for the VECTOR curve were obtained during the crystallization experiment while the data for the PROFILE curve were obtained while replaying the videotaped experiment.

polymers. Spherulite growth rate is obtained directly by monitoring the evolving scattering pattern. The average spherulite size is calculated as a function of time from the changing scattering angle of maximum intensity. The bulk crystallization rate may be determined by monitoring the overall intensity as a function of time, since intensity is directly related to the degree of crystallinity. If spherulite impingement occurs, the nucleation density can be calculated directly. If impingement does not occur, the nucleation density may also be calculated directly, assuming that heterogeneous nucleation occurs. Application of the device has been demonstrated by measuring spherulite growth rates for PET of 24700 number-average molecular weight over the temperature range 130°–200°C. This device has proven to be a powerful tool for rapidly and routinely measuring the spherulite growth rate, bulk crystallization rate, and nucleation rate/density of polymers. Recent and future software improvements will only enhance the versatility and usefulness of the device. Data obtained using the RTSALS device will be useful in guiding the development of proper polymer processing procedures for producing materials with optimum mechanical and optical properties.

The authors wish to thank Dr. J. T. Moore for helpful discussions during the course of this work.

REFERENCES

1. R. S. Stein and J. J. Keane, *J. Polym. Sci.*, **17**, 21 (1955).
2. J. J. Keane and R. S. Stein, *J. Polym. Sci.*, **20**, 327 (1956).
3. F. H. Norris and R. S. Stein, *J. Polym. Sci.*, **27**, 87 (1958).
4. R. S. Stein and M. B. Rhodes, *J. Appl. Phys.*, **31**, 1873 (1960).
5. R. J. Samuels, *J. Polym. Sci. A-2*, **9**, 2165 (1971).
6. V. G. Baranov, B. Zhu-Chan, T. I. Volkov, and S. Ya. Frenkel, *Vysokomol. Soedin. Ser. A*, **9**, 81 (1967).
7. C. Picot, G. Weill, and H. Benoit, *J. Polym. Sci. C*, **16**, 3973 (1968).
8. V. G. Baranov, A. V. Kenarov, and T. I. Volkov, *J. Polym. Sci. C*, **30**, 271 (1970).
9. K. Baba, M.S. thesis, University of Massachusetts, Amherst, 1972.
10. A. Misra, Ph.D. thesis, University of Massachusetts, Amherst, 1974.
11. R. S. Stein and A. Misra, *J. Polym. Sci., Polym. Phys. Ed.*, **11**, 109 (1973).
12. F. van Antwerpen, Ph.D. thesis, Delft Technical University, Delft, The Netherlands, 1971.
13. F. van Antwerpen and D. W. van Krevelen, *J. Polym. Sci., Polym. Phys. Ed.*, **10**, 2423 (1972).
14. R. J. Tabar, R. S. Stein, and M. B. Long, *J. Polym. Sci., Polym. Phys. Ed.*, **20**, 2041 (1982).
15. R. J. Tabar, R. S. Stein, and D. E. Rose, *J. Polym. Sci., Polym. Phys. Ed.*, **23**, 2059 (1985).
16. R. J. Tabar, P. Leite-James, and R. S. Stein, *J. Polym. Sci., Polym. Phys. Ed.*, **23**, 2085 (1985).
17. M. Ree, T. Kyu, and R. S. Stein, *J. Polym. Sci., Polym. Phys. Ed.*, **25**, 105 (1987).
18. L. J. Effler, D. N. Lewis, and J. F. Fellers, in *Polymer Association Structures*, ACS Symposium Series No. 384, American Chemical Society, Washington, D.C., 1987.
19. R. S. Stein and G. L. Wilkes, in *Structure and Prop-*

erties of Oriented Polymers, I. M. Ward, ed., Applied Science, 1975.
20. G. L. Wilkes, *J. Macromol. Sci., Rev.,* **C10,** 149 (1974).
21. R. S. Stein, A. Misra, T. Yuasa, and F. Khambatta, *Pure Appl. Chem.,* **49,** 915 (1977).
22. J. S. Higgins and R. S. Stein, *J. Appl. Cryst.,* **11,** 346 (1978).
23. J. D. Hoffman, G. T. Davis, and J. I. Lauritzen, Jr., *Treatise on Solid State Chemistry,* Vol. 3, Chap. 7 Plenum, New York, 1976.
24. M. B. Rhodes and R. S. Stein, *J. Appl. Phys.,* **39,** 4903 (1968).
25. J. T. Yeh and J. Runt, *J. Polym. Sci., Polym. Phys. Ed.,* **27,** 1543 (1989).
26. R. S. Stein, C. Picot, M. Mategi, and H. Kawai, *J. Polym. Sci. A-2,* **8,** 2115 (1970).
27. C. Picot and R. S. Stein, *J. Polym. Sci. A-2,* **8,** 2127 (1970).
28. R. S. Stein and W. Chu, *J. Polym. Sci. A-2,* **8,** 1137 (1970).
29. T. Hashimoto and R. S. Stein, *J. Polym. Sci. A-2,* **9,** 1747 (1971).
30. G. H. Meeten and P. Navard, *J. Polym. Sci., Polym. Phys. Ed.,* **22,** 2159 (1984); *ibid,* **27,** 2023 (1989); *ibid,* **27,** 2037 (1989).
31. D. Turnbull and J. C. Fisher, *J. Chem. Phys.,* **17,** 71 (1949).
32. M. Avrami, *J. Chem. Phys.,* **7,** 1103 (1939); *ibid,* **8,** 212 (1940); *ibid,* **9,** 177 (1941).
33. J. H. Magill, *Polymer,* **2,** 221 (1961).
34. J. Koberstein, T. P. Russell, and R. S. Stein, *J. Polym. Sci., Polym. Phys. Ed.,* **17,** 1719 (1979).

Received November 4, 1991
Accepted March 9, 1992